International Journal of Nanomedicine

Dovepress
Taylor & Francis Group

Open Access Full Text Article

ORIGINAL RESEARCH

Functionalized Carbon Dots With Intrinsic Wnt/β-Catenin Inhibition to Synergistically Promote 5-Fluorouracil Chemotherapy

Ziwei Yang[1], Mingyue Zhou[1], Tianpeng Yin[2], Cai-Yun Wang[1], Guo-Yuan Zhu[1], Li-Ping Bai[1], Zhi-Hong Jiang[1], Wei Zhang[1]

[1]State Key Laboratory of Quality Research in Chinese Medicine, Macau University of Science and Technology, Taipa, Macau, People's Republic of China; [2]Biomedical Research and Development Center, Zunyi Medical University, Zhuhai, People's Republic of China

Correspondence: Zhi-Hong Jiang; Wei Zhang, Macau University of Science and Technology, Taipa, Macau, 999078, People's Republic of China, Email zhjiang@must.edu.mo; wzhang@must.edu.mo

Background: 5-fluorouracil (5-FU) is the most widely used anti-pyrimidine drug that exerts its cytotoxic effect by causing DNA damage. The Wnt/*β*-catenin pathway has been considered a promising strategy to improve chemosensitivity by enhancing the DNA damage response of chemotherapy drugs. Combination therapies against cancers could inevitably affect endogenous levels of ribonucleotides (RNs) and deoxyribonucleotides (dRNs) which are critical for DNA synthesis and repair. However, exploring satisfactory Wnt/*β*-catenin inhibitors for synergistic therapy through regulating RNs and dRNs remains challenging.

Methods and Results: Here, *aloe vera*-derived carbon dots (A-CDs) with good bioactivity were synthesized via a one-step hydrothermal process, demonstrating both intrinsic Wnt/*β*-catenin inhibition and bioimaging capabilities to overcome the limitations of conventional Wnt/*β*-catenin inhibitors. The as-prepared A-CDs were further served as the transport vehicle for 5-FU, facilitating synergistic combination therapy by inhibiting the Wnt/*β*-catenin pathway, which could possibly accelerate nucleotide imbalance of dATP, ATP, TMP, and dUMP, ultimately leading to enhanced 5-FU efficiency. Additionally, the tumor-targeted material (HA-CDs @5-FU) was synthesized by modifying hyaluronic acid (HA) onto CDs@5-FU and exhibited superior antitumor efficacy in vivo with negligible side effects.

Conclusion: Overall, this study provided a novel strategy for Wnt/*β*-catenin inhibition and synergistic therapy, providing insights into the application of nano-agents in cancer therapy.

Keywords: carbon dots, Wnt/β-catenin, nucleotide metabolism, DNA damage, synergistically effects

Introduction

5-fluorouracil (5-FU), the first synthesized antimetabolite, is the most widely used anti-pyrimidine drug in clinical treatment.[1,2] The cytotoxicity of 5-FU has been ascribed to cause DNA damage.[2,3] The Wnt/*β*-catenin pathway is a conserved signaling axis participating in diverse physiological processes such as proliferation, differentiation, apoptosis, migration, invasion and tissue homeostasis. Increasing evidence indicates that dysregulation of the Wnt/*β*-catenin contributed to the development and progression of some solid tumors.[4,5] Moreover, recent studies demonstrate that Wnt/*β*-catenin components including FZD5, GSK-3*β*, and *β*-catenin play a role in regulating DNA repair factors, and silencing them can lead to decreased DNA repair and enhanced DNA damage in cancer cells.[4–6] Thus, targeting the Wnt/*β*-catenin signaling pathway has emerged as a promising approach to achieve improvements in combined chemotherapy.[7,8]

The combination therapy could inevitably affect endogenous levels of RNs and dRNs that are essential for a variety of cellular processes.[9–11] It has been well characterized that the reduction or imbalance in RNs and dRNs levels is known to result in uncontrolled DNA replication, which plays an important role in transformation and tumor progression.[12,13] However, the exact impact of RNs and dRNs under this combination therapy is yet to be fully elucidated. Moreover, the systemic toxicity and low tumor specificity of conventional Wnt/*β*-catenin inhibitors cannot be avoided,[14–16] exploring

Received: 14 November 2024
Accepted: 22 January 2025
Published: 13 February 2025

a satisfactory method to inhibit Wnt/*β*-catenin pathway is beneficial to provide an understanding of potential nucleotide metabolism in combined therapy.

Bioactive nanomaterials have gained growing interest in biology owing to their unique bioactivity and nanomaterial properties, including low toxicity, facile preparation, and ability to undergo targeted modifications.[17–19] If nanoparticles could be applied in Wnt/*β*-catenin inhibition strategies, it would be of higher value in combinational therapies. Among these nanoparticles, carbon dots (CDs) have garnered considerable attention due to their small size, robust fluorescence properties, and excellent biocompatibility.[20–26] Furthermore, some CDs prepared from the biomass may maintain the similar properties of their precursors and potentially increase new biological activities,[27–30] which conferring diverse pharmaceutical properties to CDs in cancer therapy. Therefore, these accomplishments inspire us to develop a novel CD-based strategy to overcome the limitations of conventional Wnt/*β*-catenin inhibitors in combinational therapies. As demonstrated in our previous research, *Aloe vera* exhibited inhibitory activity against the Wnt/*β*-catenin signaling pathway.[31] Therefore, utilizing *aloe vera* as the precursor for CDs could combine the advantages of both *aloe vera* and CDs, which is meaningful to the development of nano-Wnt/*β*-catenin inhibitor.

In this study, the novel A-CDs with intrinsic Wnt/*β*-catenin inhibition capacity were synthesized from *aloe vera* via a one-step hydrothermal method, offering a new approach to inhibit Wnt/*β*-catenin by integrating biological function and nanomaterial properties. Moreover, A-CDs were utilized as the transport vehicle for 5-FU, facilitating synergistic combination therapy by suppressing the Wnt/*β*-catenin pathway, resulting in promoting DNA damage through intracellular RN and dRN metabolic regulation. Hyaluronic acid (HA) coated CDs@5-FU complexes (HA-CDs@5-FU) were designed to achieve tumor-specific targeting (Graphical Abstract). Our research aimed to provide novel ideas of Wnt/*β*-catenin inhibitors for achieving better synergistic chemotherapy. Additionally, elucidating the mechanism of combination therapy through intracellular RNs and dRNs metabolic regulation might provide a new perspective on effective tumor therapy.

Materials and Method

Materials

5-FU (purity > 99%) was s supplied by from GuangZhou Lide Biotechnology Co. (Guangdong, China). Medicinal *aloe vera* L. (*A*. barbadensis Miller) was obtained from the market, Zhuhai. Hyaluronic acid (HA), N-Hydroxysuccinimide (EDC), and N-Hydroxy succinimide (NHS) were purchased from GuangZhou Lide Biotechnology Co. (Guangdong, China). The Wnt/*β*-catenin inhibition ability was determined by Steady-glo®luciferase assay system kit (Promega Corporation, Madison, USA). 3-(4,5-dimethylthiazol-2-yl)-2,5-diphenyltetrazolium bromide (MTT) was provided by Sigma-Aldrich Inc. (St. Louis, USA). The ultrapure water was prepared using a Milli-Q Gradient water system (Millipore, Bedford, MA, USA).

Preparation of A-CDs

Medicinal *aloe vera* components were determined by LC-MS/MS method. Among of them, aloesin (1.21 ± 0.27 ng/mL), aloenin (1.96 ± 1.01 ng/mL), aloin B (25.59 ± 3.61 ng/mL), and aloin A (25.11 ± 4.09 ng/mL) were the main components of *aloe vera*. Then, *aloe vera* was used as the precursor to prepare A-CDs through a one-pot solvothermal method. Specifically, *aloe vera* (0.5 g) was dissolved in 8 mL ultrapure water. Next, the mixture was transferred into a 25 mL stainless-steel autoclave vessel. After heating at 240 °C for 6 h, the mixtures were filtered with a Millipore filter (0.22 μm) to remove insoluble impurities. Finally, the obtained solution of 8 mL was dialyzed for 48 h against the deionized water of 2 L, with the deionized water being changed every 12 h until the deionized water was colorless. The A-CDs were then collected and freeze-dried for further usage.

Preparation of CDs@5-FU/HA-CDs@5-FU

CDs@5-FU Synthesis

Five milligrams of 5-Fu was incubated with 10 mL of A-CDs (1 mg mL^{-1}) solution at 37 °C for 24 h, the product was obtained by dialyzing 24 h to remove non-conjugated 5-FU. Finally, the solution was freeze-dried to obtain solid CDs@5-FU.

HA-CDs@5-FU synthesis. 2 mg HA was added in 5mL CDs@5-FU solution (2mg mL^{-1}) and incubated for another 24 h. Then, the synthesized nanoparticles were collected through dialyzing with water. Finally, the synthesized HA-CDs @5-FU had been freeze-dried and stored for further use.

To evaluate 5-FU loading efficiency in nanomaterials, the amount of free drug outside of the dialysis membrane was measured by a UV-vis spectrophotometry at 266 nm and calculated using a calibration curve of pure 5-FU. The drug loading capacity was assessed using the following equations. Drug loading capacity = (total drug added − free non-conjugated drug)/(total weight of nanomaterials) × 100%.

Characterization of NPs

Transmission electron microscopy (TEM, JEOL, FEI, Tokyo, Japan) was used to observe the morphology and structure of nanoparticles. A-CDs were dispersed in anhydrous ethanol and subjected to ultrasonic treatment. Then, the ultrasonic dispersion sample was dropped on a copper mesh and observed under TEM.

Fourier transform infrared spectroscopy (FTIR, STA6000-TL9000-Clarus SQ8 analyzer, PerkinElmer, Waltham, MA, USA) was used to evaluate the functional groups of nanoparticles. The sample powder was mixed with potassium bromide powder in a mortar under an infrared lamp and then pressed into a transparent sheet on the tablet pressing machine. FTIR spectrometer was used to record the spectra, the infrared spectral resolution is 4 cm^{-1}, the scanning range is 4000–400 cm^{-1}, and the scanning times are 32.

Fluorescence spectrophotometer (Hitachi F-4600 spectrophotometer, Hitachi, Japan) was performed to determine the fluorescence intensity of nanoparticles. A-CDs were diluted in water (500 ug mL^{-1}) and measured. The fluorescence spectra excited ranging from 300 to 400 nm with an interval of 10 nm using excitation and emission slit widths of 5 nm.

ZS90 ZetaSizer Nano series (Malvern Instruments Ltd., UK) was used to determine the zeta potential of the nanoparticles. The water-soluble sample was placed in 40 μL Malvern Micro Sample Pool (Cuvette Cell, ZEN0040) for analysis. The Zetasizer Software was used to evaluate the zeta potential of nanoparticles.

X-ray photoelectron spectroscopy (XPS) was performed on a thermo scientific K-Alpha XPS system (Thermo Fisher Scientific, UK) to investigate the element composition for nanoparticles.

Confocal laser scanning microscope (CLSM, Leica SP8, Wetzlar, Germany) was used to take cell images.

5-FU Release From Nanomaterials

In brief, 40 mg of CDs@5-FU or HA-CDs@5-FU were dissolved in 4 mL of deionized water and transferred to dialysis bags, which were subsequently immersed in 400 mL of PBS buffer (pH 6.8) in an incubator (37 °C, 400 rpm), respectively. At the scheduled intervals (10, 30, 60, 120, 240, 360, 480, 600,1440, 2160 min), 2 mL suspension was taken out from each group and replaced with the same quantity of fresh PBS buffer.[32] The collected aliquots were analyzed with a UV-vis spectrophotometer at 266 nm. All measurements were separately performed in triplicate.

Cell Culture

NIH/3T3 cells stably transfected with a Super TCF (STCF) reporter gene plasmid were obtained from Curegenix Inc (Guangzhou, China). HCT 116 cells (human colon cancer cells), LLC-1 cells (Lewis lung carcinoma cells), HT-29 cells (human colon adenocarcinoma cells), and normal LO2 cells (human hepatic cell lines LO2) were purchased from Guangzhou Lide Biotechnology Co. (Guangdong, China). NIH/3T3, HT-29, LLC-1 and LO2 cells were cultured in Dulbecco's modified Eagle's medium (DMEM) containing 10% FBS, 100 U mL^{-1} penicillin and 100 μg mL^{-1} streptomycin in a 5% CO_2 humidified incubator at 37 °C. HCT 116 cells were cultured in McCoy's 5A Medium containing 10% FBS, 100 U mL^{-1} penicillin, and 100 μg mL^{-1} streptomycin in a humidified atmosphere of 5% CO2 at 37 °C. The medium was changed every 2–3 days.

Cell Cytotoxicity Assay

Cytotoxicity Assays of A-CDs: HCT 116, HT-29, LLC-1 and LO2 cells at a density of 4×10^4 cells mL^{-1} were seeded into each well of a 96-well plate and cultured overnight. Then, the medium was removed, and 100 μL of medium containing different concentrations of *A-CDs* (12.5, 25, 50,100, 200, and 300 μg mL^{-1}) was added to each well. After 24h, 48h, and

72 h incubation, 10 μL of MTT (5 μg mL^{-1}) was added to each well and incubated for another 4 h. Finally, the medium was replaced with 150 μL dimethyl sulfoxide, and a microplate reader (Infinite M200 PRO, Tecan, Salzburg, Austria) was used to measure the absorbance at a wavelength of 490 nm. The cell viability was presented as a percentage of the control group.

Cytotoxicity Assays of nanoparticles: HCT 116, HT-29, LLC-1 and LO2 cells were cultivated in 96-well plates at a density of 4×10^4 cells mL^{-1} and allowed to adhere overnight. Subsequently, 5-FU, CDs@5-FU, and HA-CDs@5-FU (with equivalent concentration to free 5-FU) were added to each well for suitable incubation. Eventually, MTT assay was used to measure the cell viability, and IC_{50} values were calculated as mean ± SD.

Wnt/β-Catenin Inhibiting Activity

The Wnt/*β*-catenin signaling inhibitory activity of *aloe vera* and A-CDs was assessed using a luciferase reporter assay.[31] First, NIH/3T3 cells at a density of 2×10^4 cells were seeded onto 96-well plates per well for 24 h. Next, the culture medium was exchanged with fresh medium containing different concentrations of drugs (*aloe vera* and A-CDs for 0–400 ug mL^{-1}) and Wnt3a protein solution (100 ng mL^{-1}) for another 24 h. After washed twice with PBS solution, the cells were exposed to 30 μL of Steady-Glo@ assay reagent per well for 5 minutes at room temperature. Luciferase activities were measured using a fluorescence spectrophotometer reader.

LC-MS/MS Analysis

LLC-1 cells at a density of 2×10^6 cells were cultivated per dish in 10 cm petri dishes for 24 h. Next, 0.5 μM of 5-FU, CDs@5-FU, and HA-CDs@5-FU (with equivalent concentration to free 5-FU) was added to each dish for another 24 h. The cells were re-suspended and twice washed with ice-cold PBS before collection and counting. Cell pellets were subsequently treated with 150 μL of 80% methanol that contained 2 μM of both AMP-13C10,15N5 and ATP-13C10,15N5. The sample preparation process and endogenous RNs and dRNs measurement were carried out according to the previously established protocol on a Thermo Fisher TSQ LC-MS/MS system (Thermo Fisher, San Jose, CA, USA).

Western Blotting of LLC-1 Cells

LLC-1 cells were seeded in a 6-well plate and cultured overnight. The medium was then replaced with 2 mL medium containing A-CDs (100 μg mL^{-1}), 5-FU, CDs@5-FU, and HA-CDs@5-FU (with equivalent concentration to free 5-FU of 0.5 μM) for another 24 h. The protein extracts were run on SDS-PAGE and then transferred on transferred onto PVDF membranes (Millipore). The blot was blocked with 5% BSA for 1 h at room temperature and incubated with primary antibodies overnight at 4 °C. The following primary antibodies were used: anti-GAPDH ((ab8235, 1:1000 (Abcam)), *β*-catenin ((ab6302), 1:1000 (Abcam)), cyclin D1 ((ab134175), 1:1000 (Abcam)), and γ-H2AX ((ab26350), 1:1000 (Abcam)). Afterward, secondary antibodies were added and incubated for 2 h at room temperature. And secondary antibodies including anti-rabbit IgG (# 7074P2) and anti-mouse IgG (# 7076P2) were obtained from Cell Signaling Technology Inc. (Boston, MA, USA).[33] After final washing, the signal was detected with chemiluminescence reagent by Amersham Imager 600, and the band density was analyzed by Quantity One software (Version 4.6.2, Bio-Rad, USA).

LLC-1 Tumor Treatment in Vivo

C 57 mice (6–8 weeks old, female) were purchased from Guangdong Medical Laboratory Animal Centre (Guangzhou, China). All animal experiments were performed in accordance with the Guidelines for the Animal Inspection and Control of Macau and were approved by the Animal Care and Use Committee of Macau University of Science and Technology.

LLC-1 cells (1×10^7 mL^{-1}, 100 μL) were implanted into the backs of mice to establish a cancer model. Chemotherapy was initiated when the tumor volume reached 50–100 mm^3. Tumor-bearing mice were randomly divided into four groups (six mice per group) and treated with PBS, 5-FU, CDs@5-FU, and HA-CDs@5-FU, respectively (with a 5-FU equivalent of 12.5 mg kg^{-1}). Five injections were administered in total from day 10 to day 25, at two-day intervals. The tumor volume and body weight of mice were monitored every three days to evaluate the antitumor activities and systematic toxicities of nanomaterials. The tumor volume (V) was calculated according to the formula: $V = L\times W^2/2$, where L is the

largest tumor diameter and W is the smallest tumor diameter. At the end of the experiment, all the mice were sacrificed, and the tumors were collected for weighing, hematoxylin and eosin (H&E) staining and Western blotting.

Statistical Analysis

All data were presented as mean ± standard deviation (SD). The difference between groups was determined by the *T* test (GraphPad Prism 9.0 software) and one-way ANOVA (SPSS 23.0 software). $*p < 0.05$, $**p < 0.01$, and $***p < 0.001$ were considered to be statistically significant.

Results and Discussion

Preparation and Characterization of A-CDs

In this work, A-CDs were successfully prepared from *aloe vera* via the hydrothermal method. As shown in Figure 1a, the TEM image confirms that A-CDs were well dispersed, and their diameters are mainly in the range of 3–5 nm. The corresponding HRTEM image (Figure 1b) shows 0.25 nm lattice fringes, which is ascribed to the (100) crystal plane of graphitic carbon.[20,34] The UV-vis absorption spectrum of A-CDs exhibited an obvious absorption band at 280 nm (Figure 1c), which was attributed to the π-π transition of the sp^2 domains.[20] As shown in the inset of Figure 1c and Figure S1, the photographs of A-CDs solution display yellow transparent under sunlight and strong blue fluorescence under UV radiation at 365 nm. And the fluorescence quantum yield of the A-CDs was measured to be 9.3% using quinine sulfate as standard. To further understand the PL character of A-CDs, the PL excitation and emission spectra of A-CDs with different wavelengths were recorded. As shown in Figure 1d, the PL spectra excited ranging from 300 to 400 nm with an interval of 10 nm show excitation-dependent fluorescence. Additionally, the optimal excitation wavelength of A-CDs is 330 nm with a maximal fluorescence emission peak position at 450 nm, as depicted in Figure 1c.

The excellent optical properties of A-CDs indicated their potential as a fluorescent probe for cell imaging applications.[34–36] To validate this hypothesis, LLC-1 cells were subjected to A-CDs at non-toxic concentrations (300 μg mL^{-1}) for 4 h, followed by observation via CLSM. As shown in Figure 1e, considering that excitation at 405, 488, and 561 nm results in blue, green, and red fluorescence emissions, respectively, the synthesized A-CDs could effectively label the cells under varying light irradiation conditions and identify the precise localization of CDs within the cells. Moreover, the longer the incubation time corresponded to enhanced fluorescence intensity, indicating that cellular uptake occurred in a time-dependent manner.

To investigate the element composition for A-CDs, XPS survey was performed. As shown in the XPS full scan spectrum in Figure 2a, the A-CDs mainly consist of carbon, nitrogen, and oxygen. The high-resolution C 1s XPS spectrum (Figure 2b) exhibits four peaks at 283.78, 284.68, 286.48, and 288.08 eV, which are corresponding to C-C/C=C, C-N, C-O, and C=O, respectively.[20,22] The N1s XPS spectrum (Figure 2c) shows two peaks at 398.28 and 400.48 eV, which belonged to N-H and C-N, respectively. The O1s XPS spectrum (Figure 2d) involved two peaks at 531.28 and 532.78 eV, which belong to the C=O and C-O bonds, respectively.[20,37] The FTIR spectrum in Figure 2e shows the functional groups on the surface of A-CDs. The absorption bands at around 3020–3720 cm^{-1} correspond to the stretching vibrations of OH/NH. The peak at 1630 cm^{-1} reflects the absorption of C=O bonds of COOH, CHO, and CONH. The peak at 1390 cm^{-1} and 1120 cm^{-1} belongs to the C-N and C-O groups, respectively.[20,37] The analysis of the FTIR spectrum is consistent with the results of the XPS spectrum, revealing that synthesized A-CDs possess abundant functional groups on their surface, which endowed A-CDs with negative zeta potential of ≈10 mV (Figure 2f). The structural characteristics and small particle size of A-CDs substantiated their potential biological significance.

Bioactivity of A-CDs

The cellular effect of A-CDs was assessed on LO2, LLC-1, HT-29, and HCT 116 cells. As shown in Figure 2g and Figure S2, over 80% of cells remained viable after exposure to increasing concentrations of A-CDs up to 100 μg mL^{-1} for 72 h, demonstrating the exceptional biocompatibility of A-CDs in cancer therapy.

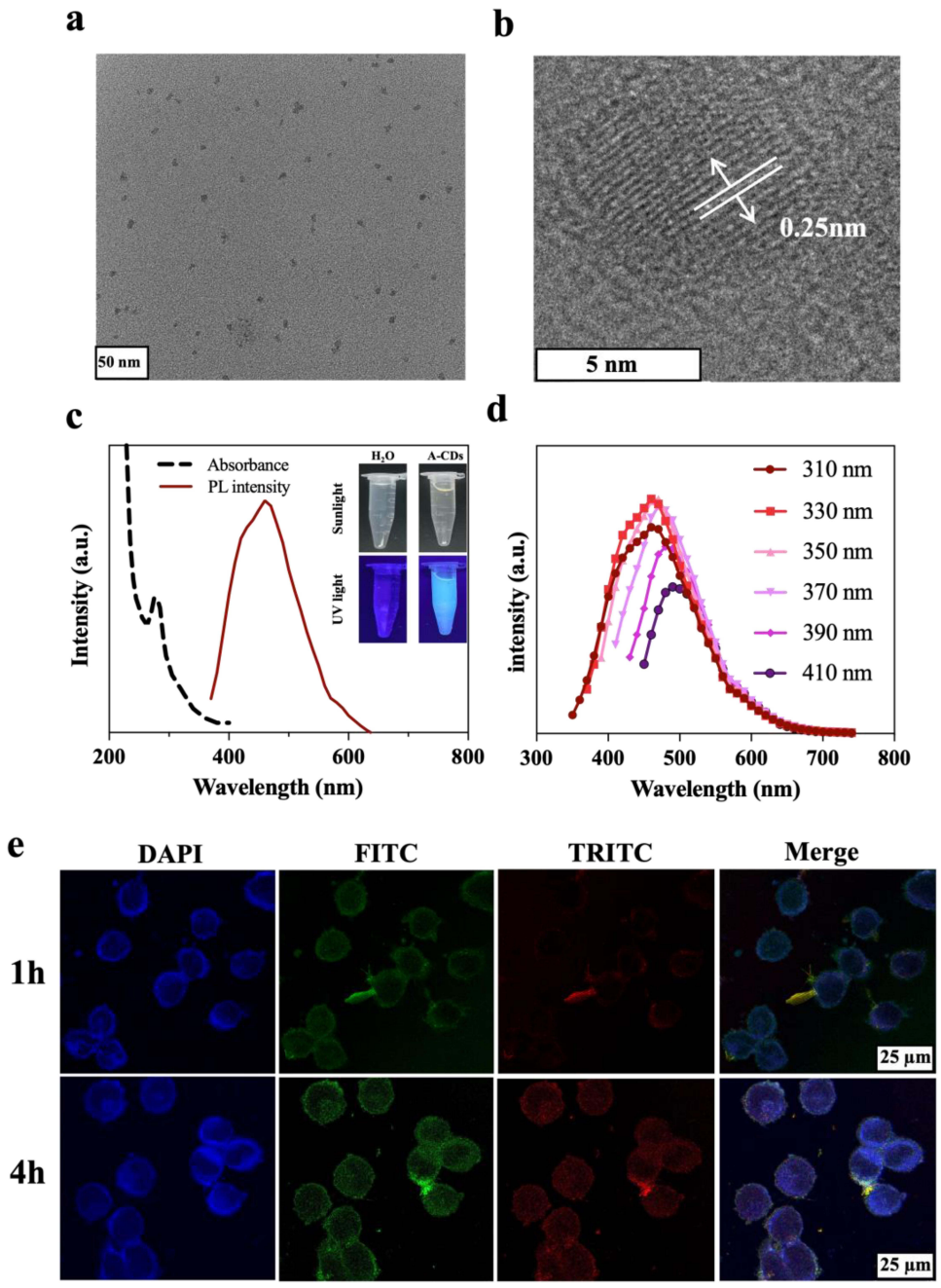

Figure 1 Characteristics of A-CDs. (**a**) TEM, (**b**) HRTEM, and (**c**) UV-vis absorption (black) and PL emission spectra (red) of A-CDs; (**d**) PL excitation dependent spectra of A-CDs; (**e**) CLSM images of LLC-1 cells incubated with A-CDs for 1h and 4 h in fluorescence radiation at 405 nm, 488 nm, 561 nm, and merge field (scale bar = 25 μm).

Wnt/β-Catenin Signaling Inhibition Activities of A-CDs

To evaluate whether A-CDs could preserve the biological activity of *aloe Vera*, we investigated the influence of *aloe vera* and A-CDs on Wnt/*β*-catenin signaling pathway through the luciferase reporter gene assay. As shown in Figure 2h, the activation of Wnt/*β*-catenin was weakened as the concentration of A-CDs increased, which eventually converted to an inhibitory effect when reaching a certain concentration, indicating that A-CDs could inhibit Wnt/*β*-catenin signaling. In addition, to clarify the synergistic effect of A-CDs, we evaluated the combinatorial effects of A-CDs and 5-FU at various concentrations on cancer cells. As demonstrated in Figure S3, the proliferation of LLC-1, HT-29, and HCT 116 cells was suppressed when pretreated with A-CDs (at a concentration of 100 μg mL^{-1}) compared to free 5-FU treatment. These

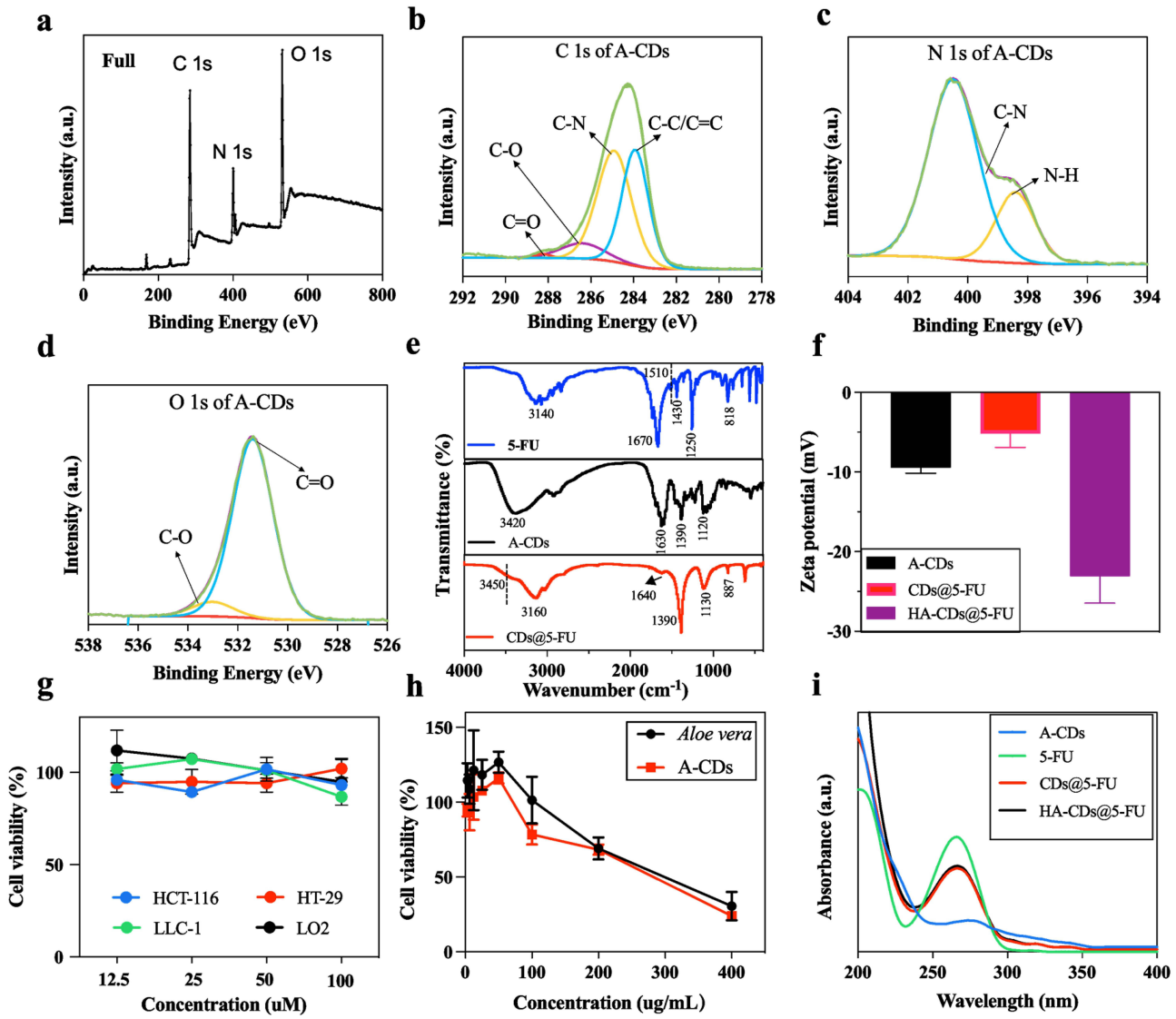

Figure 2 (**a**) Full scan XPS survey spectrum of A-CDs; High-resolution spectra of A-CDs for (**b**) C 1s, (**c**) N 1s, and (**d**) O 1s; (**e**) FTIR spectra of A-CDs, 5-FU, and CDs@5-FU; (**f**) Zeta potential of A-CDs, CDs@5-FU, and HA- CDs@5-FU;) (**g**) Cell viability of HCT 116, HT-29, LLC-1, and LO2 cells treated with A-CDs 72h (n = 4); (**h**) Wnt/*β*-catenin signaling pathway inhibition activities of A-CDs and *aloe vera* by luciferase reporter gene assay (n = 3); (**i**) UV-vis absorption spectra of 5-FU, A-CDs, CDs@5-FU, and HA-CDs@5-FU aqueous solution.

data presented here provided convincing evidence for A-CDs could retain the biological activity and synergistic efficacy of *aloe vera*.

Drug Loading and Drug Release of CDs@5-FU and HA-CDs@5-FU

The A-CDs were expected to load and deliver drugs for cancer therapy. 5-FU, the most widely used anti-pyrimidine drug, was selected for such investigation.[1,2] First, the standard absorbance curve of 5-FU was established by a UV-vis spectrophotometry at 266 nm. As showed in supplemented Figure S4, the absorbance intensity and concentration of 5-FU drugs showed a good linear relationship (R^2=0.99). Then, 5-FU loading efficiency (in weight) of the CDs@5-FU was determined to be approximately 4.7% using the calibration curve of pure 5-FU. The FTIR spectra of bare 5-FU (Figure 2e) showed the characteristic peaks of 5-FU at 3140 cm^{-1}, 1670 cm^{-1}, 1510 cm^{-1}, 1430 cm^{-1}, 1250 cm^{-1}, and 818 cm^{-1}, corresponding to N-H stretching, C=O stretching, N-H bending, C-N stretching, C-F stretching, and C-H bending, respectively.[38–40] As seen from Figure 2e, the FTIR spectrum of CDs@5-FU showed peaks of A-CDs and 5-FU at 3450 cm^{-1}, 3160 cm^{-1}, 1640 cm^{-1}, 1390 cm^{-1},

https://doi.org/10.2147/IJN.S503540

1130 cm^{-1}, and 887cm^{-1}, suggesting the successful binding of 5-FU. There were no new peaks detected in the CDs@5-FU spectrum, indicating 5-FU conjugated with A-CDs through non-covalent interactions. Since 5-FU contains a double C=C bond, thus it may bind with A-CDs through π-π interactions.[38,39] In addition, the UV spectrum of CDs@5-FU (depicted in Figure 2i) showed a clear peak at 266 nm, suggested the successful loading of 5-FU. The formation of CDs@5-FU was further investigated by H-NMR spectrometry (Figure S5a-5c). The chemical shift at 7.7 ppm in Figure S5a corresponds to the aromatic hydrogen atoms of 5-FU, which had also been observed in CDs@5-FU (Figure S5c), verifying the successful loading of 5-FU.

HA has a special affinity for CD44 receptors that are overexpressed on the surface of tumor cells,[41,42] consequently prompting the further modification of CDs@5-FU with HA to achieve tumor-specific targeting. The 5-FU loading efficiency (in weight) of the HA-CDs@5-FU was determined to be approximately 4.3%. It must be mentioned that CDs@5-FU exhibited negative charge value (−5.2 mV, Figure 2f) as calculated from zeta potential measurement. After binding of negative HA with the prepared CDs@5-FU, the zeta potential value changed to −23.1 mV (Figure 2f), suggesting that the interaction is non-electrostatic. The FTIR spectrum of HA-CDs@5-FU was showed in Figure S6. The peak at 3410 cm^{-1} corresponds to the hydroxyl characteristic peak was shifted and increased in HA-CDs@5-FU compared to CDs@5-FU, probably due to the hydrogen bonding between the hydroxyl groups of HA-CDs@5-FU. This behavior was similar to other HA coated nanomaterials.[43,44] To investigate the in vitro drug release profile of the prepared nanomaterials, CDs@5-FU and HA-CDs@5-FU were selected as carrier models and exhibited similar release trends in phosphate buffer solution (pH 6.8). As illustrated in Figure S7, approximately 60% of 5-FU was released from CDs@5-FU and HA-CDs@5-FU within 240 min due to the migration of loosely attached drugs from the surface into the release medium,[21] followed by a sustained release of 90% until 36 h. The in vitro release profile of the free 5-FU solution, CDs@5-FU and HA-CDs@5-FU was also examined in phosphate buffer solution (PH 7.4) and presented in Figure S8. The result clearly showed approximately 90% of 5-FU was available in the PBS buffer within the first 2 h, suggesting that 5-FU does not aggregate and can trespass the dialysis bag membrane. Moreover, within the first 2 h, the burst release of 5-FU from CDs@5-FU and HA-CDs@5-FU was approximately 47% and 48%, respectively. Therefore, both CDs@5-FU and HA-CDs@5-FU displayed good sustained-release behaviors.

Cytotoxicity Study in vitro

We further explored the combinatorial synergistic effects of CDs@5-FU and HA-CDs@5-FU against cancer cells in vitro by MTT assay. LLC-1, HT-29, and HCT 116 cells were exposed to various concentrations of 5-FU, CDs@5-FU, and HA-CDs@5-FU (each having an equivalent amount of 5-FU). As illustrated in Figure 3a–c, both CDs@5-FU and HA-CDs @5-FU displayed dose-responsive cytotoxicity with enhanced inhibitory effects for LLC-1, HT-29, and HCT 116 cells. Moreover, the calculated IC_{50} values (available in Table S1, supplementary information) of CDs@5-FU and HA-CDs @5-FU were obvious lower than that of free 5-FU, implying they had a synergistic cytotoxic effect on cancer cells. Furthermore, the HA-CDs@5-FU treatment showed the most prominent inhibitory effect compared to free 5-FU and CDs@5-FU treatments, which could be ascribed to the presence of HA, with a specific binding affinity for CD44 receptors,[41,42] thereby realizing targeted tumor recognition.

To investigate the cytotoxicity of nanomaterials against normal cells, LO2 cells were subjected to various concentrations of 5-FU, CDs@5-FU, and HA-CDs@5-FU (each having an equivalent quantity of 5-FU) for 48 h. The results (Figure 3d) demonstrated that all groups exerted similar inhibitory effect on the growth of LO2 cells, indicating that CDs@5-FU and HA-CDs@5-FU would not increase the drug toxicity to normal cells.

Nanomaterials Lead to the Perturbation of RNs and dRNs Pools

For gaining detail insight into the complex intracellular metabolic changes triggered by DNA damage, we employed the targeted LC/MS-MS method[45,46] to analyze the alterations in these metabolomics profiles of CDs@5-FU and HA-CDs@5-FU treated cells. Treatment with 5-FU resulted in an expected increase in ATP and dATP levels, which was similar to the literature published before[12,13] (Table S2, Table S3). 5-FU could incorporate into RNA synthesis or interference with DNA synthesis (Figure S9), which may be responsible for the accumulation of ATP and

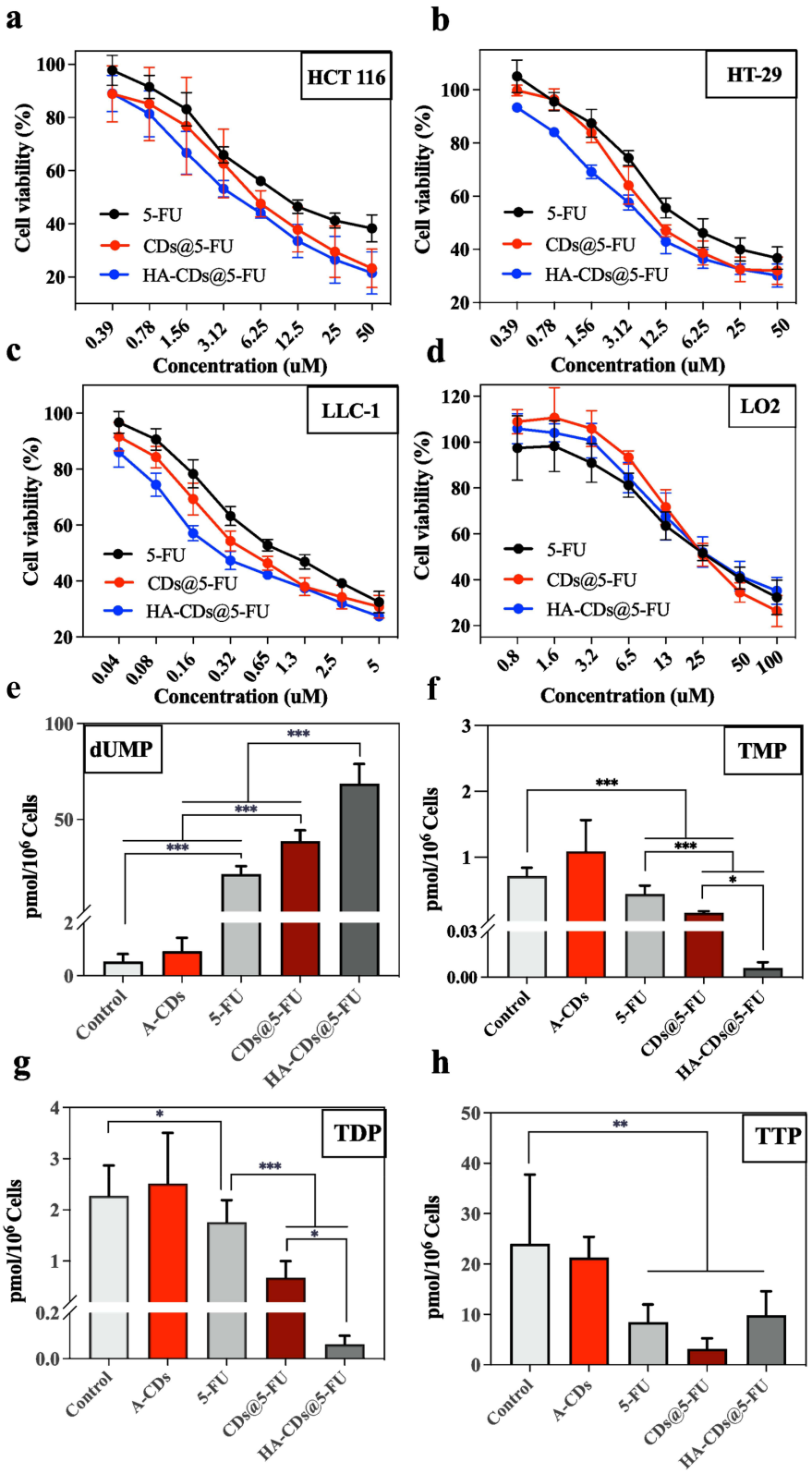

Figure 3 Cell viability of (**a**) HCT 116 for 48 h, (**b**) HT-29 cells for 72 h, (**c**) LLC-1 cells for 48 h, and (**d**) LO2 cells for 48 h treated 5-FU, CDs@5-FU, and HA-CDs@5-FU (n = 4); (**e**) dUMP, (**f**) TMP, (**g**) TDP, and (**h**) TTP contents of LLC-1 cells treated with 5-FU, A-CDs, CDs@5-FU, and HA-CDs@5-FU for 24 h (n = 6). *$p < 0.05$, **$p < 0.01$, and ***$p < 0.001$.

https://doi.org/10.2147/IJN.S503540

dATP.[12,13] Compared to single 5-FU treatment, the combination therapies of CDs@5-FU and HA-CDs@5-FU resulted in obvious increases in ATP and dATP levels, with dATP levels rising from 2 to 8 or even 15 folds. It suggested that the perturbations of ATP and dATP were more sensitive after the combinational administration, potentially exacerbating the nucleotide imbalance and significantly inhibiting DNA and RNA synthesis, leading to enhanced 5-FU efficiency.

5-FU as a DNA synthesis inhibitor and its active metabolite 5-fluoro-2′-deoxyuridine-5′-monophosphate (FdUMP) could inhibit thymidylate synthase (TS), which methylates dUMP to TMP. Interrupting the action of this enzyme would lead to the inhibition of TMP synthesis, accumulation of dUMP, depletion of deoxythymidine metabolites, and ultimately affecting DNA synthesis[1,2] (Figure S9). As expected, 5-FU treatment showed an expected elevation in dUMP levels (Figure 3e) but presented the contrary tendency in TTP, TDP, and TMP (Figure 3f–h), revealing that 5-FU induced DNA damage on LLC-1 cells. Upon exposure to CDs@5-FU treatment, dUMP level was notably higher than that under single 5-FU treatment, whereas TTP, TDP, and TMP were lower. These findings indicated that combinational treatment might induce more profound DNA damage compared to single 5-FU treatment. Taken together, CDs@5-FU could increase DNA damage, and the enhanced DNA damage might be associated with the aggravated imbalance of ATP, dATP, TMP, and dUMP. Furthermore, HA-CDs@5-FU treatment exhibited the most drastic imbalance in RNs and dRNs, suggesting that HA-CDs@5-FU could potentially cause the most severe DNA damage, which corroborated the results obtained from in vitro MTT experiments.

Inhibition of Wnt/β-Catenin-Related Gene Expression

Since 5-FU cause DNA damage during the DNA replication process, we measured the γ-H2AX level (a marker of DNA DSB) in LLC-1 cells via Western blot analysis.[1,2] The results (displayed in Figure 4a and b) indicated that treatment with CDs@5-FU and HA-CDs@5-FU could significantly increase the γ-H2AX level compared to free 5-FU, demonstrating the enhanced DNA damage to nanomaterials. These findings suggested the synergistic effects of CDs@5-FU and HA-CDs@5-FU were relative with DNA damage, which was consistent with RNs and dRNs content changes.

It is well known that the Wnt/*β*-catenin is an important oncogenic signal pathway in relation to tumor proliferation, which is activated in Lewis lung cancer.[47–49] To further understand the synergistic mechanism of nanomaterials, we aimed to investigate whether the enhanced antitumor effects of the CDs@5-FU and HA-CDs@5-FU were associated with the Wnt/*β*-catenin pathway. Western blot analysis (Figure 4a, c and d) demonstrated that LLC-1 cells exposed to A-CDs for 24 h experienced a notable reduction in protein levels of *β*-catenin and its associated target genes Cyclin D1, implying A-CDs might inhibit the Wnt/*β*-catenin pathway in LLC-1 cells. Moreover, treatment with CDs@5-FU and HA-CDs@5-FU effectively reduced *β*-catenin and Cyclin D1 levels compared to the single 5-FU treatment, suggesting that the synergistic effect of CDs@5-FU and HA-CDs@5-FU is partly mediated by the suppression of Wnt/*β*-catenin, which may be ascribed to the existence of A-CDs.

Antitumor Activity in Vivo

In order to evaluate the therapeutic effect of CDs@5-FU and HA-CDs@5-FU in vivo, four experimental groups of LLC-1 tumor-bearing mice model were given a dose of 12.5 mg 5-FU equivalent/kg body weight or PBS every three days (Figure 5a). The body weights of all groups showed a normal range and displayed a slight rising trend without significant differences (Figure 5b), indicating that CDs@5-FU and HA-CDs@5-FU did not cause serious side effects during the treatment period. Tumor volume was shown in Figure 5c, mice treated with PBS and 5-FU presented an obvious rapid tumor growth, while those treated with nanomaterials were more slowly, which was ascribed to intrinsic Wnt/*β*-catenin inhibition of A-CDs, leading to a more effective antitumor effect. Additionally, the mice treated with HA-CDs@5-FU exhibited the most pronounced tumor inhibition, which could be attributed to the cancer-targeting property of HA that enables HA-CDs@5-FU to enter cells more effectively. As shown in Figure 5d and e, tumor weight and morphology of each group directly demonstrated a superior therapeutic efficacy of HA-CDs@5-FU group, followed by CDs@5-FU treated group.

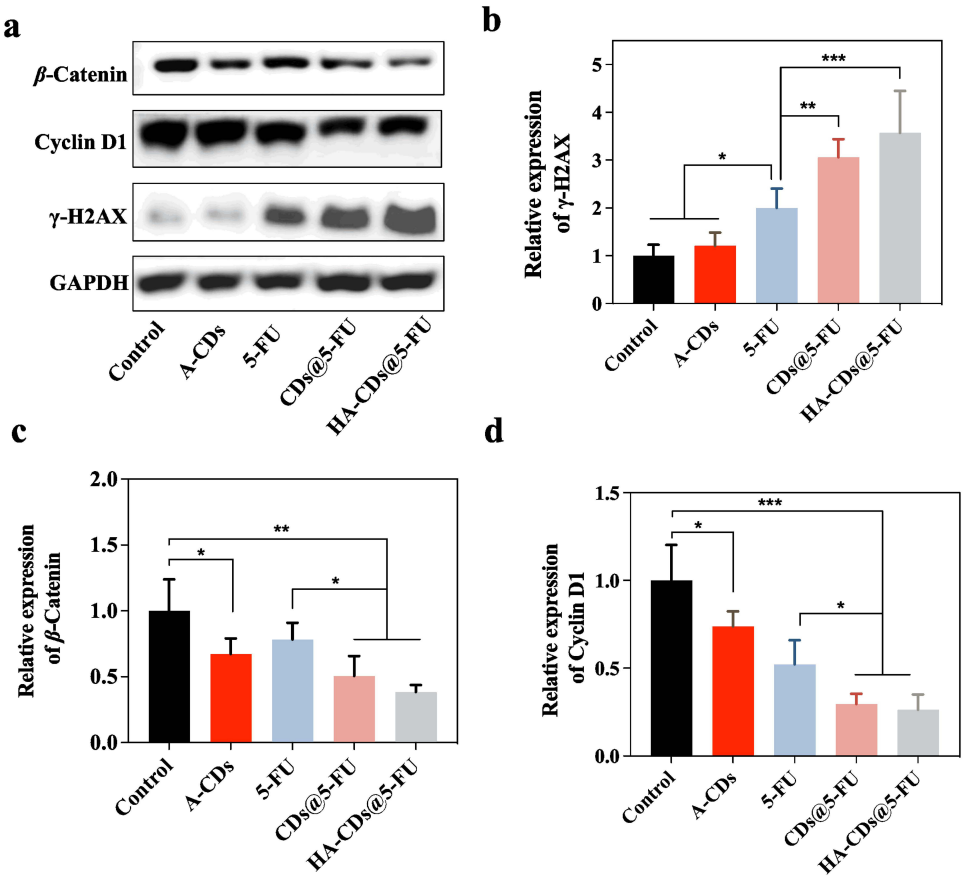

Figure 4 (**a**) Western blotting analysis showing the expression levels of (**b**) γ-H2AX, (**c**) *β*-catenin, and (**d**) cyclin-D1 in LLC-1 cells after 24 h incubation (n = 4). **p* < 0.05, ***p* < 0.01, and ****p* < 0.001.

To further verify the antitumor mechanism of nanomaterials on tumors, the expression of γ-H2AX, *β*-catenin and cyclin-D1 were evaluated through Western blotting in the PBS, 5-FU, CDs@5-FU, and HA-CDs@5-FU experimental groups (Figure 5f–g). The lower expression levels of *β*-catenin and cyclin-D1 were observed in CDs@5-FU and HA-CDs @5-FU groups compared to free 5-FU group, suggesting that nanomaterials could effectively inhibit Wnt/*β*-catenin in vivo. In addition, the highest γ-H2AX level was observed in the HA-CDs@5-FU-treated group, followed by CDs@5-FU-treated group, indicating CDs@5-FU and HA-CDs@5-FU could induce the more severe DNA compared to single 5-FU treatment. These results were consistent with the corresponding tumor inhibition effect, confirming that the synergistic effect of nanomaterials was related to the enhanced DNA damage in vivo. Collectively, these results indicated that CDs@5-FU and HA-CDs@5-FU augmented Wnt/*β*-catenin inhibition and DNA damage in animal model, achieving a synergistic effect.

The tumor tissues were also sectioned into slices for H&E staining. As illustrated in Figure 5h, the more extensive apoptotic cells were observed in CDs@5-FU and HA-CDs@5-FU treated tumor tissues, revealing the remarkable synergistic therapeutic efficacy of nanomaterials. For the toxicity evaluation in vivo, the major organs of the treated mice were also subjected to H&E staining (Figure S10), which showed no significant cytoarchitectural alterations or inflammatory lesions in the detected organs, further demonstrating the reliable safety of CDs@5-FU and HA-CDs@5-FU.

https://doi.org/10.2147/IJN.S503540

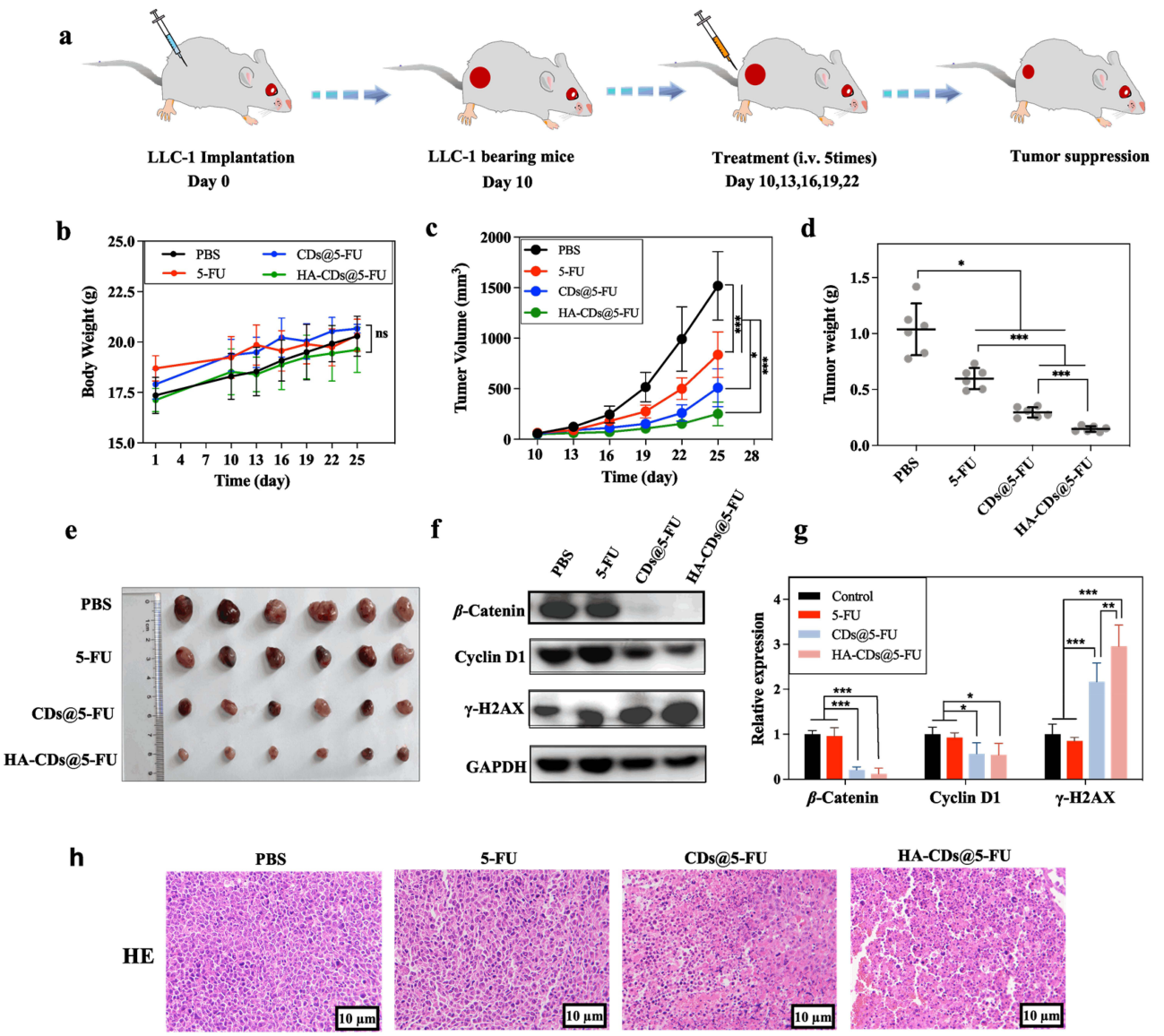

Figure 5 Antitumor effect of nanomaterials in mice. (**a**) Schematic illustration in *vivo* therapy; (**b**) The body weight changes, (**c**) relative tumor growth curves, and (**d**) tumor weight after different treatments in mice (n = 6); (**e**) The tumor photographs after the administration. (**f** and **g**) Western blotting analysis showing the levels of γ-H2AX, *β*-catenin, and cyclin-D1 in tumors with PBS, 5-FU, CDs@5-FU, and HA-CD@5-FU treatments (n = 4); (**h**) Representative H&E staining images of tumors excised from LLC-1 bearing mice after 25 days of treatments (Scale bars: 10 μm). **p* < 0.05, and ***p* < 0.01, and ****p* < 0.001.

Conclusion

A combination chemotherapy strategy based on Wnt/*β*-catenin inhibition involving nucleotide metabolism was designed in the study. The novel A-CDs were designed by a facile hydrothermal treatment of *aloe vera*, which displayed intrinsic Wnt/*β*-catenin inhibition, favorable biocompatibility and good cell imaging ability. More importantly, a functional CD-based drug delivery system (CDs@5-FU) with intrinsic Wnt/*β*-catenin inhibition ability was developed for synergistic therapy, which could possibly improve 5-FU sensitivity by accelerating the nucleotide imbalances of dATP, ATP, dUMP, and TMP, leading to enhanced DNA damage. This 5-FU delivery system (CDs@5-FU) highlights the unique advantages of Wnt/*β*-catenin self-inhibition in synergistic therapy and makes up for the drawback that reported 5-FU nanocarriers have no therapeutic efficacy. Furthermore, HA was conjugated with CDs@5-FU to create a targeted anticancer nano-platform. The established HA-CDs @5-FU demonstrated excellent anti-tumor effect and favorable biocompatibility, with no apparent tissue toxicity observed in vivo. Therefore, these findings highlight that A-CDs hold great potential as a multifunctional nanocarrier for Wnt/*β*-catenin

inhibition and synergistic therapy. The explanation of intracellular nucleoside metabolism could also provide new ideas for effective combination treatments.

Acknowledgments

This work was supported by grants from the Macau Science and Technology Development Fund (0001/2023/AKP, 0051/2024/RIA1 and 006/2023/SKL).

Author Contributions

All authors made a significant contribution to the work reported, whether that is in the conception, study design, execution, acquisition of data, analysis and interpretation, or in all these areas; took part in drafting, revising or critically reviewing the article; gave final approval of the version to be published; have agreed on the journal to which the article has been submitted; and agree to be accountable for all aspects of the work.

Disclosure

The authors declare no conflict of interest.

References

1. Longley DB, Harkin DP, Johnston PG. 5-fluorouracil: mechanisms of action and clinical strategies. *Nat Rev Cancer*. 2003;3:330–338. doi:10.1038/nrc1074
2. Sethy C, Kundu CN. 5-Fluorouracil (5-FU) resistance and the new strategy to enhance the sensitivity against cancer: implication of DNA repair inhibition. *Biomed Pharmacother*. 2021;137:111285. doi:10.1016/j.biopha.2021.111285
3. Sancar A, Lindsey-Boltz LA, Unsal-Kacmaz K, et al. Molecular mechanisms of mammalian DNA repair and the DNA damage checkpoints. *Annu Rev Biochem*. 2004;73:39. doi:10.1146/annurev.biochem.73.011303.073723
4. Zhang Y, Wang X. Targeting the Wnt/beta-catenin signaling pathway in cancer. *J Hematol Oncol*. 2020;13:165. doi:10.1186/s13045-020-00990-3
5. Karimaian A, Majidinia M, Bannazadeh BH, et al. The crosstalk between Wnt/beta-catenin signaling pathway with DNA damage response and oxidative stress: implications in cancer therapy. *DNA Repair*. 2017;51:14–19. doi:10.1016/j.dnarep.2017.01.003
6. Zhang X, Yu X. Crosstalk between Wnt/beta-catenin signaling pathway and DNA damage response in cancer: a new direction for overcoming therapy resistance. *Front Pharmacol*. 2023;14:1230822. doi:10.3389/fphar.2023.1230822
7. Lohiya G, Katti DS. A synergistic combination of niclosamide and doxorubicin as an efficacious therapy for all clinical subtypes of breast cancer. *Cancers*. 2021;13:3299. doi:10.3390/cancers13133299
8. Yang P, Liu W, Fu R, et al. Cucurbitacin E chemosensitizes colorectal cancer cells via mitigating TFAP4/Wnt/beta-catenin signaling. *J Agric Food Chem*. 2020;68. doi:10.1021/acs.jafc.0c05551
9. Meuth M. The molecular basis of mutations induced by deoxyribonucleoside triphosphate pool imbalances in mammalian cells. *Exp Cell Res*. 1989;181:305–316. doi:10.1016/0014-4827(89)90090-6
10. Weinberg G, Ullman B, Martin DW. Mutator phenotypes in mammalian cell mutants with distinct biochemical defects and abnormal deoxyribonucleoside triphosphate pools. *Proc Natl Acad Sci*. 1981;78:2447–2451. doi:10.1073/pnas.78.4.2447
11. Chabosseau P, Buhagiar-Labarchede G, Onclercq-Delic R, et al. Pyrimidine pool imbalance induced by BLM helicase deficiency contributes to genetic instability in Bloom syndrome. *Nat Commun*. 2011;2:368. doi:10.1038/ncomms1363
12. Li Y, Luo W, Zhang H, et al. Antitumor mechanism of hydroxycamptothecin via the metabolic perturbation of ribonucleotide and deoxyribonucleotide in human colorectal carcinoma cells. *Molecules*. 2021;26:4902. doi:10.3390/molecules26164902
13. Guo JR, Li Z, Wang CY, et al. Profiling of ribonucleotides and deoxyribonucleotides pools in response to DNA damage and repair induced by methyl methanesulfonate in cancer and normal cells. *Oncotarget*. 2017;8:101707–101719. doi:10.18632/oncotarget.21521
14. Urushibara S, Tsubota T, Asai R, et al. WNT/beta-catenin signaling inhibitor IC-2 suppresses sphere formation and sensitizes colorectal cancer cells to 5-fluorouracil. *Anticancer Res*. 2017;37:4085–4091. doi:10.21873/anticanres.11795
15. Pan F, Shen F, Yang L, et al. Inhibitory effects of XAV939 on the proliferation of small-cell lung cancer H446 cells and Wnt/beta-catenin signaling pathway in vitro. *Oncol Lett*. 2018;16:1953–1958. doi:10.3892/ol.2018.8790
16. Amerizadeh F, Rahmani F, Maftooh M, et al. Inhibition of the Wnt/b-catenin pathway using PNU-74654 reduces tumor growth in in vitro and in vivo models of colorectal cancer. *Tissue Cell*;2022. 101853. doi:10.1016/j.tice.2022.101853
17. Zhao Y, Zhang Z, Pan Z, et al. Advanced bioactive nanomaterials for biomedical applications. *Exploration*. 2021;1:20210089. doi:10.1002/EXP.20210089
18. Tan MC, Chow GM, Ren L, et al. Inorganic nanoparticles for biomedical applications. *Nanosci Biomed*. 2009;2009:272–289.
19. Mattinzoli D, Cacioppo M, Ikehata M, et al. Carbon dots conjugated to SN38 for improved colorectal anticancer therapy. *Mater Today Bio*. 2022;16:100286. doi:10.1016/j.mtbio.2022.100286
20. Xu Y, Wang B, Zhang M, et al. Carbon dots as a potential therapeutic agent for the treatment of cancer-related anemia. *Adv Mater*. 2022;34:2200905. doi:10.1002/adma.202200905
21. Horo H, Saha M, Das H, et al. Synthesis of highly fluorescent, amine-functionalized carbon dots from biotin-modified chitosan and silk-fibroin blend for target-specific delivery of antitumor agents. *Carbohydr Polym*. 2022;277:118862. doi:10.1016/j.carbpol.2021.118862
22. Wang J, Qiu J. A review of carbon dots in biological applications. *J Mater Sci*. 2016;51:4728–4738. doi:10.1007/s10853-016-9797-7
23. Kumar M, Chinnathambi S, Bakhori N, et al. Biomass-derived carbon dots as fluorescent quantum probes to visualize and modulate inflammation. *Sci Rep*. 2024;14:12665. doi:10.1038/s41598-024-62901-7

24. Bartkowski M, Zhou Y, Nabil Amin Mustafa M, et al. CARBON DOTS: bioimaging and anticancer drug delivery. *Chemistry*. 2024;30:e202303982. doi:10.1002/chem.202303982
25. Wang Y, Wu R, Zhang Y, et al. One-step synthesis of N, S-doped carbon dots with green emission and their application in 4-NP detection, pH sensing, and cell imaging. *Spectrochimica Acta Part A*. 2024;308:123709. doi:10.1016/j.saa.2023.123709
26. Jia Y, Cheng Z, Wang G, et al. Nitrogen doped biomass derived carbon dots as a fluorescence dual-mode sensing platform for detection of tetracyclines in biological and food samples. *Food Chem*. 2023;402:134245. doi:10.1016/j.foodchem.2022.134245
27. Liu H, Mo L, Chen H, et al. Carbon dots with intrinsic bioactivities for photothermal optical coherence tomography tumor-specific therapy and postoperative wound management. *Adv Healthc Mater*. 2022;11:2101448. doi:10.1002/adhm.202101448
28. Liu L, Li X, Bu W, et al. Carbon dots enhance extracellular matrix secretion for dentin-pulp complex regeneration through PI3K/Akt/mTOR pathway-mediated activation of autophagy. *Mater Today Bio*. 2022;16:100344. doi:10.1016/j.mtbio.2022.100344
29. Ren C, Hao X, Wang L, et al. Metformin carbon dots for promoting periodontal bone regeneration via activation of erk/AMPK pathway. *Adv Healthc Mater*. 2021;10:2100196. doi:10.1002/adhm.202100196
30. Shao Y, Zhu C, Fu Z, et al. Green synthesis of multifunctional fluorescent carbon dots from mulberry leaves (Morus alba L.) residues for simultaneous intracellular imaging and drug delivery. *J Nanopart Res*. 2020;22:1.
31. Dai C, Liu MP, Zhang WJ, et al. A material-basis study of Aloe vera on the wnt/β-catenin signaling pathway using a knockin/knockout method with high-speed countercurrent chromatography. *RSC Adv*. 2017;7:38819–38829. doi:10.1039/C7RA06761E
32. Feng T, Ai X, Ong H, et al. Dual-responsive carbon dots for tumor extracellular microenvironment triggered targeting and enhanced anticancer drug delivery. *ACS Appl Mater Interfaces*. 2016;8:18732–18740. doi:10.1021/acsami.6b06695
33. Guo L, Huang W, Zhang S, et al. Chicken protein S gene regulates adipogenesis and affects abdominal fat deposition. *Animals*. 2022;12(16):2046. doi:10.3390/ani12162046
34. Wang H, Zhang M, Ma Y, et al. Carbon Dots derived from citric acid and glutathione as a highly efficient intracellular reactive oxygen species scavenger for alleviating the lipopolysaccharide-induced inflammation in macrophages. *ACS Appl Mater Interfaces*. 2020;12:41088–41095. doi:10.1021/acsami.0c11735
35. Fan RJ, Sun Q, Zhang L, et al. Photoluminescent carbon dots directly derived from polyethylene glycol and their application for cellular imaging. *Carbon*. 2014;71:87–93. doi:10.1016/j.carbon.2014.01.016
36. Xu D, Lin Q, Chang HT. Recent advances and sensing applications of carbon dots. *Small Methods*. 2020;4:1900387. doi:10.1002/smtd.201900387
37. Meng W, Bai X, Wang B, et al. Biomass-derived carbon dots and their applications. *Energy Environ Mater*. 2019;2:172–192. doi:10.1002/eem2.12038
38. Kaur N, Tiwari P, Kumar P, et al. Multifaceted carbon dots: toward pH-responsive delivery of 5-fluorouracil for in vitro antiproliferative activity. *ACS Appl Bio Mater*. 2023;6(7):2760–2770. doi:10.1021/acsabm.3c00228
39. Miralinaghi P, Kashani P, Moniri E, et al. Non-linear kinetic, equilibrium, and thermodynamic studies of 5-fluorouracil adsorption onto chitosan–functionalized graphene oxide. *Mater Res Express*. 2019;6(6):065305. doi:10.1088/2053-1591/ab0831
40. Feng B, Li N, Bi Y, et al. Bio-based carbon dots loaded with 5-Fu: a multifunctional drug delivery system. *J Fluoresc*. 2024;34(4):1683–1692. doi:10.1007/s10895-023-03385-y
41. Sun Q, Bi H, Wang Z, et al. Hyaluronic acid-targeted and pH-responsive drug delivery system based on metal-organic frameworks for efficient antitumor therapy. *Biomaterials*. 2019;223:119473. doi:10.1016/j.biomaterials.2019.119473
42. Xiao Z, Zuo W, Chen L, et al. H_2O_2 self-supplying and GSH-depleting nanoplatform for chemodynamic therapy synergetic photothermal/chemotherapy. *ACS Appl Mater Interfaces*. 2021;13:43925–43936. doi:10.1021/acsami.1c10341
43. Chen S, Sun C, Wang Y, et al. Quercetagetin-loaded composite nanoparticles based on zein and hyaluronic acid: formation, characterization, and physicochemical stability. *J Agric Food Chem*. 2018;66(28):7441–7450. doi:10.1021/acs.jafc.8b01046
44. Ye G, Wu T, Li Z, et al. Preparation and characterization of novel composite nanoparticles using zein and hyaluronic acid for efficient delivery of naringenin. *Food Chem*. 2023;417:135890. doi:10.1016/j.foodchem.2023.135890
45. Li Z, Zhang HX, Li Y, et al. Method for quantification of ribonucleotides and deoxyribonucleotides in human cells using (Trimethylsilyl) diazomethane derivatization followed by liquid chromatography-tandem mass spectrometry. *Analy Chem*. 2019;91:1019–1026. doi:10.1021/acs.analchem.8b04281
46. Zhang H, Li Y, Li Z, et al. MTBSTFA derivatization-LC-MS/MS approach for the quantitative analysis of endogenous nucleotides in human colorectal carcinoma cells. *J Pharm Anal*. 2022;12:77–86. doi:10.1016/j.jpha.2021.01.001
47. Akiri G, Cherian MM, Vijayakumar S, et al. Wnt pathway aberrations including autocrine Wnt activation occur at high frequency in human non-small-cell lung carcinoma. *Oncogene*. 2009;28:2163–2172. doi:10.1038/onc.2009.82
48. Yang J, Chen J, He J, et al. Wnt signaling as potential therapeutic target in lung cancer. *Expert Opin Ther Targets*. 2016;20:999–1015. doi:10.1517/14728222.2016.1154945
49. Stewart DJ. Wnt signaling pathway in non-small cell lung cancer. *J Natl Cancer Inst*. 2014;106:djt356. doi:10.1093/jnci/djt356